Experimental and numerical investigation of a novel photovoltaic/thermal system using micro-channel flat loop heat pipe (PV/T-MCFLHP)

Fucheng Chen[1], Menglong Hu[1], Ali Badiei[2], Min Yu[2], Zicong Huang[1], Zhangyuan Wang[1,2,*] and Xudong Zhao[2]

[1]*School of Civil and Transportation Engineering, Guangdong University of Technology, 100 Waihuan Xi Road, Higher Education Mega Centre, Guangzhou, Guangdong Province, P.R. China, 510006;* [2]*Centre for Sustainable Energy Technologies, University of Hull, Cottingham Road, Hull, HU6 7RX*

Abstract

In this paper, a novel photovoltaic/thermal system using micro-channel flat loop heat pipe (PV/T-MCFLHP) is proposed, and the thermal and electrical performance of the system is investigated theoretically and experimentally. The variations of temperatures were analysed, and the efficiency of the system was calculated under different conditions, i.e. simulated solar radiation, water flow rate and refrigerant filling ratio. The maximum overall efficiency of the system was found to be 51.3%, the thermal efficiency 43.8% and the electrical efficiency 7.5% with the refrigerant filling ratio of 25%, simulated solar radiation of 800 W/m^2 and water flow rate of 400 L/h. Test results were compared with simulation results, and the recorded average error was 10.2%.

Keywords: PV/T-MCFLHP system; micro-channel flat heat pipe; loop heat pipe; theoretical analysis; testing

*Corresponding author: zwang@gdut.edu.cn

Received 22 September 2019; revised 13 February 2020; editorial decision 25 March 2020; accepted 25 March 2020

1 SYMBOLS DESCRIPTION

A—area (m^2);
C_p—specific heat (J/(kg•K));
D—diameter (m);
d—derivative;
f—function;
g—gravity acceleration (m^2/s);
H—latent heat (J/kg);
h—heat transfer coefficient (W/(m^2•K));
I—radiation (W/m^2);
L—length (m);
m—mass flow rate (kg/s);
M—mass (kg);
Nu—Nusselt number;
P—pressure (Pa);
P_e—power (W);
P_{pump}—power consumption by water pump (W);
Pr—Prandtl number;
Q—energy (W);
R—thermal resistance ((m^2•K)/W);
R_1—thermal resistance of the evaporator wall ((m^2•K)/W);
R_2—thermal resistance due to the evaporation of the working fluid ((m^2•K)/W);
R_3—thermal resistance of the vapour flow ((m^2•K)/W);
R_4—thermal resistance due to the condensation of the working fluid ((m^2•K)/W);
R_5—thermal resistance of the condenser wall ((m^2•K)/W);
R_6—thermal resistance due to the convection heat transfer of the cooling liquid ((m^2•K)/W);
R_v—vapour constant (kJ/(kg•K));
Re—Reynolds number;
t—temperature (K);
V—volumetric flow rate (L/h);

International Journal of Low-Carbon Technologies 2020, 15, 513–527

doi:10.1093/ijlct/ctaa019 Advance Access publication 3 May 2020

w—width (m);
W_η—uncertainty of efficiency (%);
W_M—uncertainty of refrigerant mass (kg);
W_V—uncertainty of water flow rate (L/h);
W_I—uncertainty of simulated radiation (W/m^2);
x—parameter relating to the filled liquid mass.
X0—initial refrigerant steam dryness;
XN—refrigerant steam dryness;
z—input parameters value;
∂—differential function;
α—absorption ratio;
β—packing factor;
η—efficiency;
δ—thickness (m);
λ—thermal conductivity (W/(m•K));
ρ—density (kg/m^3);
μ—dynamic viscosity (kg/(m•s));
γ—specific heat ratio;
σ—surface tension coefficient of refrigerant liquid (N/m);
θ—contact angle of the working fluid with the pipe wall;

2 SUBSCRIPTS DESCRIPTION

a—all;
air—ambient air;
BL—boiling limit;
bu—boiling bubble;
CL—capillary limit;
c—condenser;
cap—capillary;
cf—cooling fluid;
EL—entrainment limit;
ev—evaporator;
e—electricity;
FL—liquid filling mass limit;
f—silicone layer;
gr—groove;
hp—heat pipe;
i—dependent number;
in—inlet;
j—input number;
l—refrigerant liquid;
lf—liquid film;
MCFLHP—micro-channel flat loop heat pipe;
max—maximum value;
out—outlet;
PV—PV panel;
PV/T—photovoltaic/thermal;
rc—reference;
SL—sonic limit;
VL—viscous limit;
u—useful heat;
v—refrigerant vapour;
vtl—vapour collecting pipe;
wall—wall

1. INTRODUCTION

Due to global population growth and improving human comfort requirements, the global energy consumption has increased rapidly [1,2]. Many advanced energy-efficient technologies, capable of harvesting different clean energy sources, e.g. solar and wind energy [3,4], have been proposed. Among all the renewable sources, solar has been recognized as the most effective and abundant [5,6] to be used as energy source. In particular, solar energy technologies employing photovoltaic and solar thermal are the most promising ones due to clean and efficient production of electricity and heat [7,8].

According to the previous research in the solar energy field, solar energy technologies can be mainly divided into three categories: air type, water type and heat-pipe type [9]. Air-type solar energy systems use air as the heat transfer medium to absorb, convert and exchange heat [10]. Nagano *et al.* [10] introduced thermal-photovoltaic hybrid exterior wallboards using air circulation to transfer heat, maximizing the average thermal collector efficiency by up to 36.9%. The roof-integrated air-based solar energy system, which could provide domestic hot water and drying functions, was investigated by Chen *et al.* [11] where the thermal efficiency of the system reached 20%. In the case of the water type, higher efficiency values can be achieved due to the higher thermal and physical properties of the working liquid compared to air [9]. Chow *et al.* [12] analysed the performance of a building-integrated photovoltaic-enhanced water-heating system and found that the thermal and electrical efficiencies of the system were at 37.5% and 9.4%, respectively. A building heating system combined with the water-type PV/T collector was examined by Kim *et al.* [13] yielding a thermal efficiency of 30%.

However, there are some existing problems associated with the air-type and water-type solar energy systems, e.g. low heat transfer efficiency of the air/water and freezing problems of the water-type system. In order to tackle these issues, heat-pipe solar energy systems are proposed, which due to high thermal conductivity of the heat pipes are particularly suitable for use in the solar energy systems [14]. A thermosyphon-type heat pipe-based PV/T system was developed by Moradgholi *et al.* [15], which had a thermal efficiency of 45.1%. Long *et al.* [16] conducted experiments on a building integrated heat pipe photovoltaic/thermal system and reported that the annual water heating efficiency could reach 35% and achieved 315 kWh/year per unit façade surface area of electricity saving. Another photovoltaic loop heat pipe/solar-assisted heat pump water heating system was proposed by Li and Sun [17], and the system performance was analysed to quantify energy savings. Electricity consumption and CO_2 emission reductions of 79.4% and 73.9% were achieved by the investigated system.

The conventional heat pipes used in solar energy technologies had the disadvantages of not completely contacting with the flat solar collector structure, as well as the long heat transfer distance from the heat pipe condenser to the domestic hot water tank, leading to low thermal and electrical efficiencies [18]. To overcome these shortcomings, Yang *et al.* [19] suggested that heat pipe weight should be reduced with lightweight materials. Deng *et al.*

[20] proposed that conventional heat pipes had a long start-up time and reduced the thermal performance of the heat pipe for use in the solar energy system. Hou *et al.* [21] presented that conventional heat pipes did not contact with the PV panel properly. Chen *et al.* [22] also studied the performance of a sintering porous capillary wick into a micro-plate loop heat pipe that can improve heat transfer efficiency.

Based on the presented literature review, some parameters were considered as the most important variables influencing the performance of the solar energy systems, e.g. cooling fluid flow rate, solar radiation, cooling fluid temperature, wind speed and working fluid parameters. Nagano *et al.* [10] investigated different parameters and found that air (as the cooling fluid) flow rate, solar radiation and panel inclination and air temperature were the most important parameters of the solar energy systems. Chen *et al.* [11] also found that the climate conditions (including solar radiation and wind speed) played important roles in determining the thermal efficiency of the solar energy system. Jouhara *et al.* [14] considered material compatibility and working fluid temperature as the experimental parameters and proposed that the working fluid filling ratio would affect the heat transfer process. Therefore, three parameters (i.e. simulated radiation, cooling fluid flow rate and working fluid filling ratio) were studied in this paper.

In this paper, the performance of the photovoltaic/thermal system with a micro-channel flat loop heat pipe (MCFLHP) has been investigated. The system design involves a micro-channel flat heat pipe array as the evaporator and a U-type tubular heat exchanger as the condenser. In comparison with other similar studies, the key contribution aspects of the proposed system are as follows. (1) A micro-channel flat heat pipe array as the evaporator can reach higher vapour speeds within the micro-channels owing to the interior micro-grooves. The flat evaporator can also perfectly contact with the solar photovoltaic/thermal panel, which increases the contact area with the heat generation devices. (2) A U-type heat exchanger as the condenser can provide sufficient condensing contact area for heat transfer, leading to higher heat exchange efficiency. (3) Long heat transfer distance due to the loop structure is found to be applicable to the system design as it can operate with small pressure difference or temperature change. Through numerical modelling and experimental investigation, PV/T-MCFLHP system performance was tested through analysing the temperatures of PV surface and MCFLHP and calculating the electrical and thermal efficiencies of the system under different operating conditions of simulated solar radiation, water flow rate and refrigerant filling ratio. The results from the theoretical and experimental analyses were compared to predict the performance of the proposed system. This research will pro-

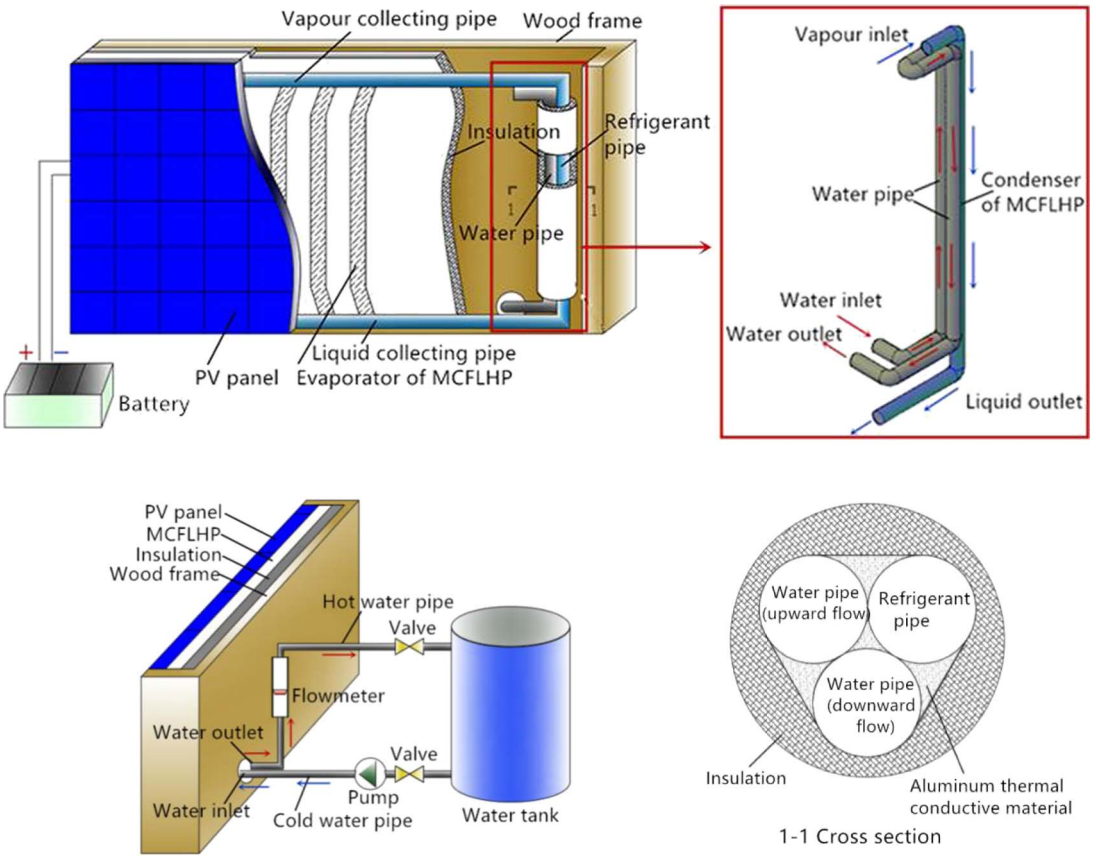

Figure 1. *Schematic of the PV/T-MCFLHP system.*

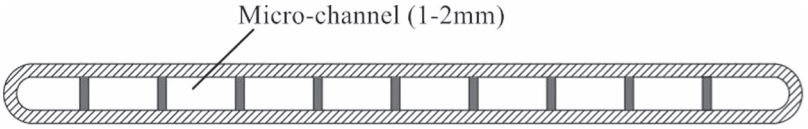

Figure 2. *Cross section of the micro-channels of the evaporator of the MCFLHP.*

vide helpful insight into potential development of advanced solar energy systems and provides the technological basis to be used in the building sector to reduce energy consumption and carbon emission, which will also be helpful for achieving the global energy saving targets.

2. SYSTEM DESCRIPTION

As seen in Figure 1, the PV/T-MCFLHP system consisted of PV panels, MCFLHP, water pipe work, water tank, water pump and a battery. The main component of the proposed system, i.e. MCFLHP, consists of an evaporator, vapour collecting pipe, condenser and liquid collecting pipe. The flat-plate evaporator of the MCFLHP was embedded between the PV panels and insulation layer, which contained independent micro-channels with a diameter of 2 mm to enhance the heat transfer (as shown in Figure 2). The vapour collecting and liquid collecting pipes were positioned above and below the evaporator to facilitate the flow of the working fluid inside the heat pipe. It should be mentioned that the working fluid inside the MCFLHP could be water or refrigerant (e.g. R134A) due to the high latent heat capacity of the working fluid. The condenser of the MCFLHP was directly connected to the U-type water pipe to enhance the heat transfer, and both were surrounded with the thermal conductive material and insulation. The water pipe was fitted with the flow meter, water tank and pump to record the water flow. The battery pack was wired to the PV panel to record the electricity generation.

The working principle of the PV/T-MCFLHP system could be summarized as follows: when the PV panel absorbs sunlight, the electricity is generated, and the excess heat from the PV panel will be transferred to the evaporator of the MCFLHP. Inside the evaporator of MCFLHP, the working fluid evaporates, and the vapour flows from the evaporator to the condenser through the vapour collecting pipe. Inside the condenser of the MCFLHP, the vapour is condensed, and the heat is released from the condenser to the water pipe to be accumulated in the water tank. As to the condensed vapour, it flows back from the condenser to the evaporator through the liquid-collecting pipe.

The key characteristics of the PV/T-MCFLHP system could be summarized as follows. (1) The micro-channel structure of the evaporator of the MCFLHP could enhance the heat transfer inside the heat pipe due to the high contact angle of the working fluid with the pipe wall, leading to improved solar-thermal conversion efficiency of the system. (2) The flat-plate structure of the evaporator of the MCFLHP improves the connection between the PV panel and the heat pipe evaporator, leading to reduced contact thermal resistance. (3) The loop heat pipe structure of the MCFLHP could separate the evaporator and condenser and therefore reduce the entrainment limit between the liquid and vapour flow inside the pipe, leading to increased heat transfer capacity and flexible installation of the system.

3. STEADY-STATE HEAT TRANSFER MODEL DEVELOPMENT FOR THE PV/T-MCFLHP SYSTEM

The steady-state heat transfer model for the PV/T-MCFLHP system is developed for the prediction of the system's performance under different structure and operating conditions.

3.1. Heat transfer limit of the MCFLHP

The heat transfer limit determining the maximum heat transfer capacity of the MCFLHP should be calculated before the development of the steady-state heat transfer model. The heat transfer limit of the MCFLHP was governed by six different limits, i.e. viscous, sonic, entrainment, capillary, boiling and liquid filling mass limits, which were directly related to the structure and operating conditions of the MCFLHP, as well as the thermal properties of the working fluids flowing inside the MCFLHP. Therefore,

$$Q_{\text{limit}} = \min\left(Q_{\text{VL}}, Q_{\text{SL}}, Q_{\text{EL}}, Q_{\text{CL}}, Q_{\text{BL}}, Q_{\text{FL}}\right) \tag{1}$$

3.1.1. *Viscous limit, Q_{VL}*

When the MCFLHP is operated at low temperature, the viscous forces in different components of the MCFLHP may be too small to drive vapour flow. Therefore, the viscous limit of the MCFLHP was the minimum of the viscous limits that occurred in the evaporator, vapour collecting pipe and condenser [23]. Taking the viscous limit in evaporator $Q_{\text{VL,ev}}$ for example,

$$Q_{\text{VL,ev}} = \frac{\pi {D_{\text{ev}}}^4 H \rho_{\text{v}} P_{\text{v}}}{256 \mu_{\text{v}} L_{\text{ev}}} \tag{2}$$

For the viscous limit within the vapour collecting pipe ($Q_{\text{VL,vtl}}$) and the condenser ($Q_{\text{VL,c}}$), the same equation can be used from Equation (2) by substituting the evaporator's parameters (e.g. diameter, length) with the equivalent inner diameter and length of the vapour collecting pipe and condenser. Thus, the smallest viscous limit values among the evaporator, vapour collecting pipe

and condenser will be the viscous limit of the system (QVL) and determined by

$$Q_{VL} = \min\left(Q_{VL,ev}, Q_{VL,vtl}, Q_{VL,c}\right) \tag{3}$$

3.1.2. *Sonic limit, Q_{SL}*

When the MCFLHP is operated at high temperature, the vapour velocity in different components of the MCFLHP may be close to the sonic or supersonic level. High-speed vapour flow would limit heat transfer capacity. Therefore, the sonic limit of the MCFLHP was the minimum of the sonic limits that occurred in the evaporator, vapour collecting pipe and condenser [24]. Taking the sonic limit in evaporator $Q_{SL,ev}$ for example,

$$Q_{SL,ev} = \left(\frac{\pi {D_{ev}}^4 H \rho_v}{4}\right)\left[\frac{\gamma_v R_v t_v}{2\left(\gamma_v + 1\right)}\right]^{0.5} \tag{4}$$

For the sonic limit within the vapour collecting pipe ($Q_{SL,vtl}$) and the condenser ($Q_{SL,c}$), the same equation can be used from Equation (4) by substituting the evaporator's parameters (e.g. diameter) with the equivalent inner diameter of the vapour collecting pipe and condenser. Thus, the smallest sonic limit values among the evaporator, vapour collecting pipe and condenser will be the sonic limit (Q_{SL}) of the system and determined by

$$Q_{SL} = \min\left(Q_{SL,ev}, Q_{SL,vtl}, Q_{SL,c}\right) \tag{5}$$

3.1.3. *Entrainment limit, Q_{EL}*

In the evaporator and condenser of the MCFLHP, when the vapour velocity was too high, the liquid would entrain into the vapour. The entrainment limit will increase fluid circulation and reduce heat transport capacity. Therefore, the entrainment limit of the MCFLHP was the minimum of the entrainment limits that occurred in the evaporator and condenser [24]. Taking the entrainment limit in evaporator $Q_{EL,ev}$ for example,

$$Q_{EL,ev} = \left(\frac{\pi {D_{ev}}^4 H}{4}\right)\left[\frac{\rho_v \sigma}{2 w_{gr}}\right]^{0.5} \tag{6}$$

For the entrainment limit within the condenser ($Q_{EL,c}$), the same equation can be used from Equation (6) by substituting the evaporator's parameters (e.g. diameter) with the equivalent inner diameter of the condenser. Thus, the smaller entrainment limit values between the evaporator and the condenser will be the entrainment limit (Q_{EL}) of the system and determined by

$$Q_{EL} = \min\left(Q_{EL,ev}, Q_{EL,c}\right) \tag{7}$$

3.1.4. *Capillary limit, Q_{CL}*

The capillary limit occurred when the capillary forces were not large enough to drive liquid circulation reflux. During operation, the capillary forces must be greater than or at least equal to total pressure drops along the MCFLHP. The maximum heat transfer capacity due to capillary limit can be written as [25]

$$Q_{CL} = \frac{\sigma_l \rho_l L_{ev}}{\mu_l} \cdot \frac{A_{hp}}{L_{gr}} \cdot \left(\frac{2}{r_{gr}} - \frac{\rho_l g L_{hp} \cos\theta}{\sigma_l}\right) \tag{8}$$

3.1.5. *Boiling limit, Q_{BL}*

When the MCFLHP operated at high temperature, the boiling limit in different components of the MCFLHP would cause a burning out of the liquid at certain areas of heat pipe wall. Therefore, the boiling limit of the MCFLHP was the minimum of the boiling limits that occurred in the evaporator and condenser [24]. Taking the boiling limit in evaporator $Q_{BL,ev}$ for example,

$$Q_{BL,ev} = \frac{2\pi L_{ev} t_v}{H \rho_v \ln\left(D_{hp}/D_{ev}\right)} \cdot \left(\frac{2}{r_{bu}} - P_{cap,max}\right) \tag{9}$$

For the boiling limit within the condenser ($Q_{BL,c}$), the same equation can be used from Equation (9) by substituting the evaporator's parameters (e.g. diameter, length) with the equivalent inner diameter and length of the condenser. Thus, the smaller boiling limit values between the evaporator and condenser will be the boiling limit (QBL) of the system and determined by

$$Q_{BL} = \min\left(Q_{BL,ev}, Q_{BL,c}\right) \tag{10}$$

3.1.6. *Liquid filling mass limit, Q_{FL}*

In order to make sure the MCFLHP working properly, a minimum liquid level in different components of the MCFLHP was required to be filled into. Liquid gravity force would affect the heat transfer capacity significantly. Therefore, the liquid filling mass limit of the MCFLHP was the minimum of the liquid filling mass limits that occurred in the evaporator [24].

$$Q_{FL} = \left(\frac{M_l}{x L_{ev}}\right)^3 \frac{\lambda_l g H}{3\pi^2 \mu_l \rho_l {D_{ev}}^2} \tag{11}$$

3.2. Heat transfer analysis

The heat transfer and energy conversion analyses of the proposed system could be summarized as three processes: (1) solar absorption process; (2) heat transfer in the MCFLHP process; and (3) heat transfer in the water pipe process. It should be mentioned that in the steady state situation, these processes stayed thermally balanced.

3.2.1. *Solar absorption process*

The solar energy absorbed by the PV panel could be written as [26, 27]

$$Q_a = \alpha_{PV} \beta_{PV} A I \tag{12}$$

Part of the absorbed energy will be converted to electricity [28, 29]:

$$Q_e = \eta_e A I \tag{13}$$

It is known that the electrical efficiency of the PV panel decreases with the increase in the PV panel's working temperature [28, 29], and this dependence is

$$\eta_e = \eta_{rc}\left[1 - \beta_{PV}\left(t_{PV} - t_{rc}\right)\right] \tag{14}$$

Part of the heat losses from the PV panel to the ambient will be determined by

$$Q_{loss} = \left(t_{PV} - t_{air}\right) 0.664 \frac{\lambda_{air}}{L_{PV}} \mathrm{Re}_{air}^{1/2} \mathrm{Pr}_{air}^{1/3} A \tag{15}$$

Therefore, the remaining part will be transferred to the MCFLHP.

$$Q_{hp} = Q_a - Q_e - Q_{loss} \tag{16}$$

3.2.2. *Heat transfer in the MCFLHP process*

This part of useful heat will be transferred from the evaporator of the MCFLHP to the condenser due to the temperature difference in between [30, 31].

$$Q_u = \frac{t_{hp} - t_{cf}}{\sum_{i=1}^{6} R_i} \tag{17}$$

$\sum_{i=1}^{6} R_i$ represents the thermal resistances from the evaporator of the MCFLHP to the cooling fluid (e.g. water) in the water pipe, which were described as follows [32]:

(1) Thermal resistance of the evaporator wall, R_1

$$R_1 = \frac{\delta_{hp}}{\lambda_{hp}} \tag{18}$$

(2) Thermal resistance due to the evaporation of the working fluid, R_2

In this process, the working fluid inside the evaporator of the MCFLHP experienced a phase change from liquid to vapour. According to the thermal conductivity of the working fluid lateral membrane, this part of thermal resistance can be written as [24]

$$R_2 = \frac{1}{h_{ev}} \tag{19}$$

h_{ev} is the evaporation heat transfer coefficient [24],

$$h_{ev} = 0.1060 \left(\frac{\lambda_l}{D_{hp}}\right)\left(\frac{\rho_l}{\rho_v}\right)^{0.128}\left(\frac{D_{hp} m_v}{\mu_l}\right)^{0.187}\left(\frac{C_p \mu_l}{\lambda_l}\right)^{0.14} \tag{20}$$

(3) Thermal resistance of the vapour flow, R_3

Vapour flow thermal resistance occurs in the vapour collecting pipe and is expressed as

$$R_3 = \frac{128 L \mu_v t_v}{\pi D^4 \rho_v{}^2 H^2} \tag{21}$$

(4) Thermal resistance due to the condensation of the working fluid, R_4

It should be mentioned that due to the direct contact of the high temperature vapour with the cold condenser wall, liquid film will be generated and attached to the inner surface of the condenser wall and form the process of the membrane condensation. In this process, the thermal resistance due to the condensation of the working fluid could be summarized as [33, 34]

$$R_4 = \frac{1}{h_{lf}} \tag{22}$$

h_{lf} is the condensation heat transfer coefficient,

$$h_{lf} = 1.13\left(\frac{\rho_l{}^2 g \lambda_l{}^3 H}{\mu_l D_c \left(t_v - t_c\right)}\right)^{\frac{1}{4}} \tag{23}$$

(5) Thermal resistance of the condenser wall, R_5

$$R_5 = \frac{\delta_{wall}}{\lambda_{wall}} \tag{24}$$

(6) Thermal resistance due to the convection heat transfer of the cooling liquid, R_6

The thermal energy will be released to the water pipe and eventually removed by the cooling liquid in the water pipe due to the convection heat transfer.

$$R_6 = \frac{D_{cf}}{\mathrm{Nu}\lambda_{cf}} \tag{25}$$

where Nu is the Nusselt number of the cooling fluid,

$$\mathrm{Nu} = 0.332 \mathrm{Re}_{cf}^{\frac{1}{2}} \mathrm{Pr}_{cf}^{\frac{1}{3}} \tag{26}$$

Re is the Reynolds number of cooling fluid, and Pr is the Prandtl number of cooling fluid.

$$\mathrm{Re}_{cf} = \frac{\rho_{cf} m_{cf} D_{cf}}{\mu_{cf}} \tag{27}$$

$$\mathrm{Pr}_{cf} = \frac{\mu_{cf} C_{p,cf}}{\lambda_{cf}} \tag{28}$$

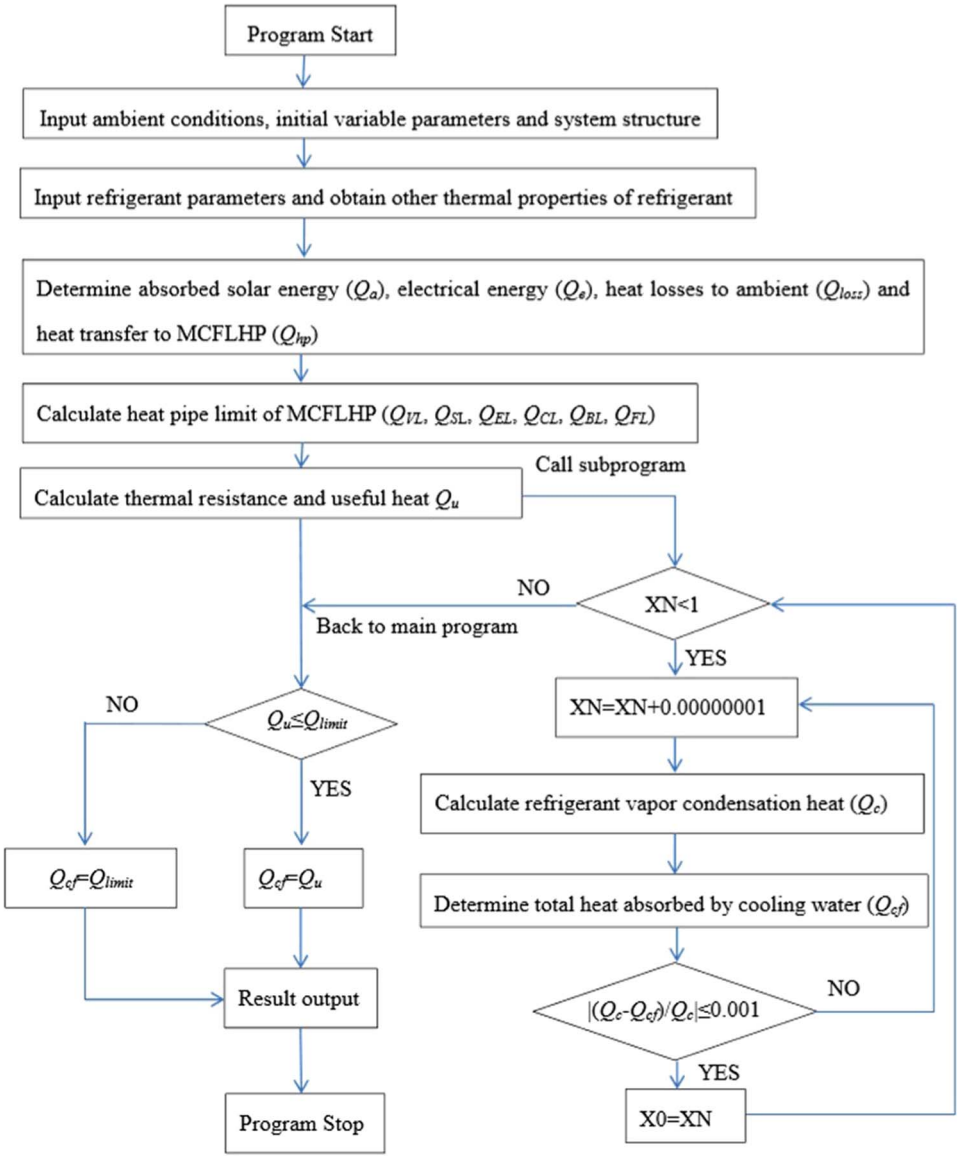

Figure 3. *Flow chart for the computational simulation of the steady-state heat transfer model.*

3.2.3. *Heat transfer in the water pipe process*

In this process, the thermal energy removed by the cooling fluid in the water pipe, Q_{cf}, could be written as

$$Q_{cf} = C_{p,cf} m_{cf} (t_{out} - t_{in}) \quad (29)$$

It should be noted that the useful heat transmitted to the cooling fluid will also depend on the heat transfer limit of the MCFLHP.If

$$Q_u > Q_{limit}, \quad Q_{cf} = Q_{limit} \quad (30)$$

If

$$Q_u \leq Q_{limit}, \quad Q_{cf} = Q_u \quad (31)$$

According to the above calculation equations, thermal efficiency of the proposed PV/T-MCFLHP system is

$$\eta_h = \frac{Q_{cf}}{Q_a} \times 100\% \quad (32)$$

3.3. Computational simulation of the steady-state heat transfer model

The flow chart for the computational simulation of the steady-state heat transfer model of the PV/T-MCFLHP system was summarized in Figure 3, and the steps are illustrated as follows:

(1) Input operating conditions, e.g. ambient temperature and ambient wind speed; initial variable parameters, e.g.

simulated solar radiation, cooling fluid flow rate; and system structure, e.g. parameters of the PV panel and MCFLHP;
(2) Input refrigerant parameters, e.g. filling ratio and working temperature, to obtain other thermal properties of refrigerant, e.g. density, dynamic viscosity;
(3) Calculate the heat transfer limit of MCFLHP (i.e. Q_{VL}, Q_{SL}, Q_{EL}, Q_{CL}, Q_{BL}, Q_{FL}) using Equations (2)–(11), and determine the governing heat transfer limit Q_{limit} using Equation (1);
(4) Determine the absorbed solar energy Q_a, electrical energy Q_e, heat losses to the ambient Q_{loss} and amount of heat transferred to the MCFLHP Q_{hp} using Equations (12)–(16);
(5) Determine the amount of heat transfer in the MCFLHP Q_u using Equations (17)–(28);
(6) Determine the heat transferred to the cooling fluid via condenser Q_{cf} using Equation (29), and the parameters of the condenser (e.g. outlet water temperature, length of condenser) based on iterative method;
(7) Compare Q_{cf} and Q_{limit}, and determine the final results of Q_{cf} using Equations (30)–(31);
(8) Calculate the output results, e.g. thermal efficiency, using Equation (32);
(9) Stop the programme.

4. EXPERIMENTAL WORK

In order to investigate the performance of the PV/T-MCFLHP system and to verify the model results, the experimental rig was constructed at the laboratory of Guangdong University of Technology, China as shown in Figure 4, following the original system design in Section 3 using the constructed model. The PV panel manufactured by Dongguan Wu Xing Company (China) had the length, width and thickness of 1500, 760 and 5 mm, respectively. The MCFLHP was custom-made and closely bonded to the back of the PV panel (by using the thermal-conductive silicone grease) to take the heat away from PV panel, which had the total contact area of 1.14 m^2. As to the evaporator of the MCFLHP, 33 micro-channel heat pipes (760-mm length, 18-mm width and 2-mm thickness) with the micro-grooves inside to improve heat transfer were used as the evaporator of the system. The filling ratio of the working fluid inside the MCFLHP was chosen at 25–35%. The vapour collecting pipe and liquid collecting pipe were designed to collect the vapour vaporized in each micro-channel heat pipe and distribute the refrigerant liquid evenly to each micro-channel heat pipe respectively, and both of them had the length of 1800 mm. The condenser of the MCFLHP was the circular tube with 20-mm diameter, and the condenser and water pipe (with 20 mm diameter) together constituted the vertical-tube counter-current heat exchanger. The PV panel and the MCFLHP were surrounded and protected by the wood frame of 2100-mm length, 1050-mm width and 105-mm thickness. Regarding the thermal storage, the 70-L water tank was installed. The water pump was used to drive water through the heat exchanger by overcoming the flow resistances. The battery was parallel connected to the PV panel for the recording of the electricity generation. The parameters of the main components of the system are shown in Table 1.

In terms of the testing equipment, a solar simulator (TRM-PD1) (shown in Figure 4b) was used to provide the simulated solar radiation, which has 12 sunlamps and a control cabinet that can adjust the simulated solar radiation arriving at the surface of the PV panel. The PV performance from the battery storage was measured by using a power sensor (i.e. PV panel data collector), which can record the output electricity (voltage and current) of the PV panel. When the amount of the simulated solar radiation or PV surface temperature changes, it can detect and measure the output electricity of the PV panel due to the change in the voltage and current of the PV panel. The water flow rate in the water pipe was controlled by the water pump and tested by the water flow meter, and the PV panel data collector collected the amount of electricity generation. The temperatures of the system components, e.g. PV panel, MCFLHP, and water tank, were recorded by the multi-channel temperature recorder with the thermocouples. The parameters of the testing equipment are shown in Table 2.

It should be noted that in order to study the operation performance of the PV/T-MCFLHP system, the total number of 31 temperatures measuring points, i.e. P1–P31, were used, and the positions of the measuring points are shown in Figure 5. P1–P10 was continuously set on the vapour collecting pipe to obtain temperature variations. P11–P16 was located in the condenser of the MCFLHP and recorded the liquid flow during the condensation process at the condenser. It was worth mentioning that P17–P19 was located in the No. 3 of the heat pipe, and P20–P22 was located in the No. 33 of the heat pipe, representing the most far and the most near evaporator heat pipe to the condenser, respectively. These three temperature-measuring points on each heat pipe measured the temperature variations in the top, centre and bottom levels of the heat pipe respectively. P23–P31 was arranged on the surface of the PV panel, measuring different temperature and simulated radiation variations.

As to the working conditions of the PV/T-MCFLHP system, three variable parameters to the system performance, i.e. simulated radiation, water flow rate and refrigerant filling ratio, were investigated and analysed. In this stage of research, the performance of the system was studied, and the experiment work was conducted under lab conditions. Therefore, the simulated radiation supplied to the system changed from 600 to 800 W/m^2, the water flow rate varied from 300 to 500 L/h and the filling ratio was chosen at 25% and 35% of the total volume inside the MCFLHP representing the refrigerant mass at 1.0 and 1.1 kg, respectively.

5. RESULTS AND DISCUSSIONS

In this section, the heat transfer analysis of the MCFLHP is presented. The thermal efficiency values from simulations and test results are compared and the electrical efficiency and total efficiency of the proposed system are calculated.

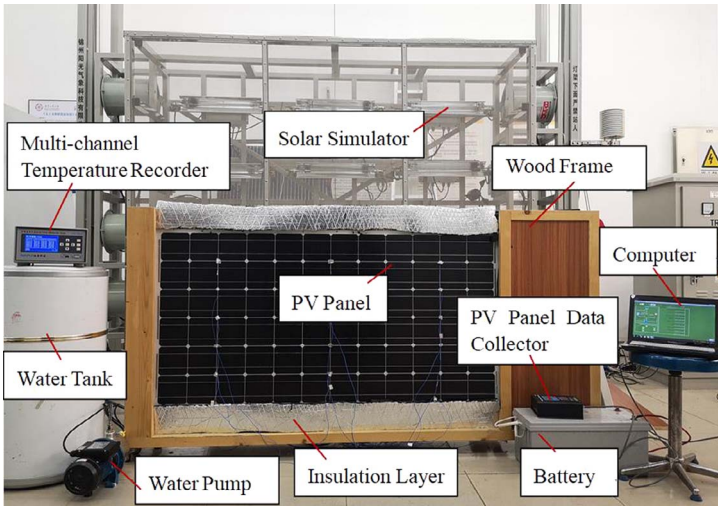

(a) Front view

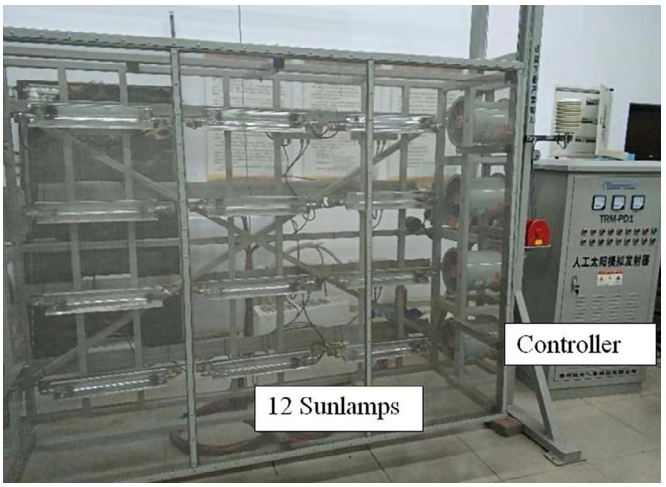

(b) Solar simulator

(c) PV panel data collector

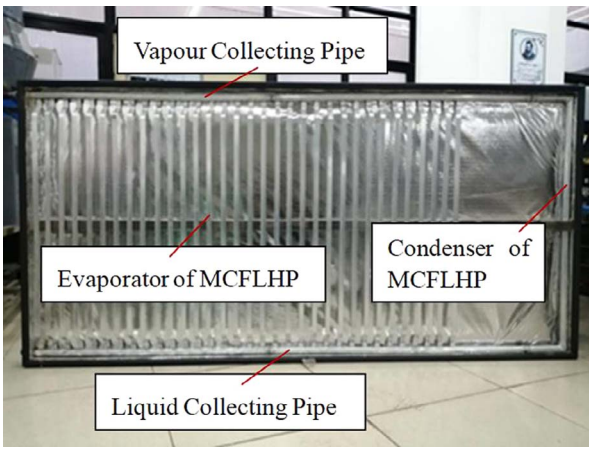

(d) Internal structure of the MCFLHP

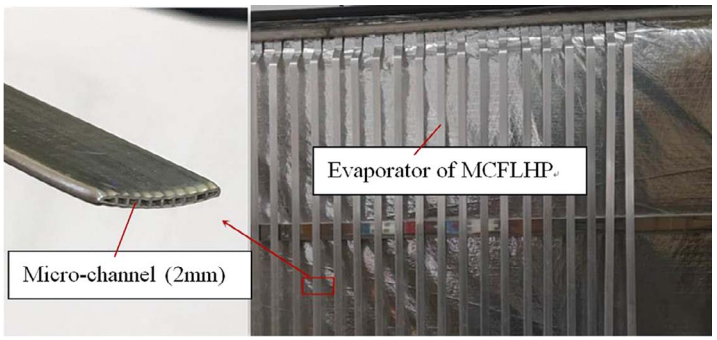

(e) Cross-section of the micro-channels

Figure 4. *Testing rig of the PV/T-MCFLHP system.*

5.1. Heat transfer analysis of the MCFLHP

The average temperature variation of the MCFLHP is shown in Figures 6–11 under the steady-state conditions. From Figures 6 and 7, it is obvious that in the vapour collecting pipe (from P1 to P10), the temperature gradually increased to the highest (at measuring point 4) and then decreased dramatically (from P11 to P16). As to the evaporator part of the heat pipe, the superheated vapour gathered at the top of the heat pipe and finally maintained the temperature reaching the highest at P4, while in the condenser (P11–P16), the transferred heat will be released to the water

Table 1. *Parameters of the system components.*

	Length (mm)	Width (mm)	Thickness (mm)	Area (m^2)	Diameter (mm)	Volume (L)
PV panel	1500	760	5	1.14	-	-
MCFLHP	760	18	2	-	-	-
Wood frame	2100	1050	105	-	-	-
Vapour collecting pipe	1800	-	-	-	20	-
Liquid collecting pipe	1800	-	-	-	20	-
Water tank	-	-	-	-	-	70

Table 2. *Parameters of the testing equipment.*

No.	Item	Model	Parameters
1	Multi-channel temperature recorder	JK-8/16 AT4532	Sensor: nickel chromium-nickel silicon (type K); Size of the sensor: 1 cm*1 cm; Temperature test range: −50∼1000°C; Measure accuracy: 0∼ ± (0.5% + 1); Power supply: 220 V ± 10%, 50 Hz ± 2%; Temperature signal input channel: 64
2	Solar simulator	TRM-PD1	Total power supply: 56 kW; Ambient temperature: 5∼35°C; Relative humidity: 75%; Error: ±6.5 W/m^2
4	PV panel data collector	MPPT	Full cut-off voltage: 13∼15 V; Charging current limit: 10∼30 A; Balanced charging time: 1∼10 h;
5	Battery		Operational temperature: −40∼ + 70°C; Charging pressure (at 25°C): 14.4∼15.0 V
7	Water flow meter	LFS25	Measurement rage: 100–1000 L/h; Accuracy level: 4; Pressure level: 4.0 MPa; Error: ±10 L/h.
8	Water pump	ORS25-10G	Voltage: 220 V; power: 60 W; head: 10 m; DN: 25 mm.
9	Power sensor	MPPT	Solar power controller MPPT

flowing across, and the temperature decreased dramatically. From the Figures 8–11, it can be seen that due to the heat absorption of the evaporator of the MCFLHP, the temperature increase in each pipe was almost the same indicating that different heat pipe evaporators evenly absorbed the simulated radiation. The temperature in the top level of the heat pipes was higher than that in the bottom level. The reason could be summarized in two aspects. First, the driving forces from the superheated vapour and liquid gravitation should overcome the flow resistance of the working fluid. Since the evaporator of the heat pipe was vertically installed, the top-level temperature was higher than the bottom-level temperature. Second, the temperature in the bottom level of the evaporator was also influenced from the condensed liquid flowing in the liquid collecting pipe.

The testing tank's water temperature increase is shown in Table 3 for the operation period of 1 h. It was found that the tank water temperature increased with the decrease in the refrigerant filling ratio and simulated radiation. After the experiments (shown in Table 3), the optimum water flow rate of the system was 400 L/h when the system was tested under the same refrigerant filling ratio of 25% and the same simulated radiation of 700 W/m^2; when maintaining the same filling ratio of 25% and the same water flow rate of 400 L/h, the system's thermal efficiency increased first and then decreased with the variation of the simulated solar radiation from 600-800 W/m^2; and the most appropriate refrigerant filling ratio of 25% was determined when the testing was conducted under the simulated solar radiation of 700 W/m^2 and water flow rate of 400 L/h.

5.2. Comparison of the system's thermal efficiency

The comparison of the simulated and testing thermal efficiency of the proposed system shows (in Table 3) that good agreement can be achieved with the acceptable average error of 10.2%. As the simulation revealed, three factors, i.e. simulated solar radiation, water flow rate and refrigerant filling ratio, have significant impact on the overall performance of the system. The average thermal efficiency of 43.8% from experiments and 48.7% from simulations were achieved with the refrigerant filling mass of 25%, simulated radiation of 700 W/m^2 and water flow rate of 400 L/h. The cause of the difference between the simulation and testing results could be identified from two aspects. From the simulation aspect, the reason may lie in the assumptions made for the simplification of the computational calculation; from the testing aspect, the reason may lie in the errors due to the testing equipment or the testing

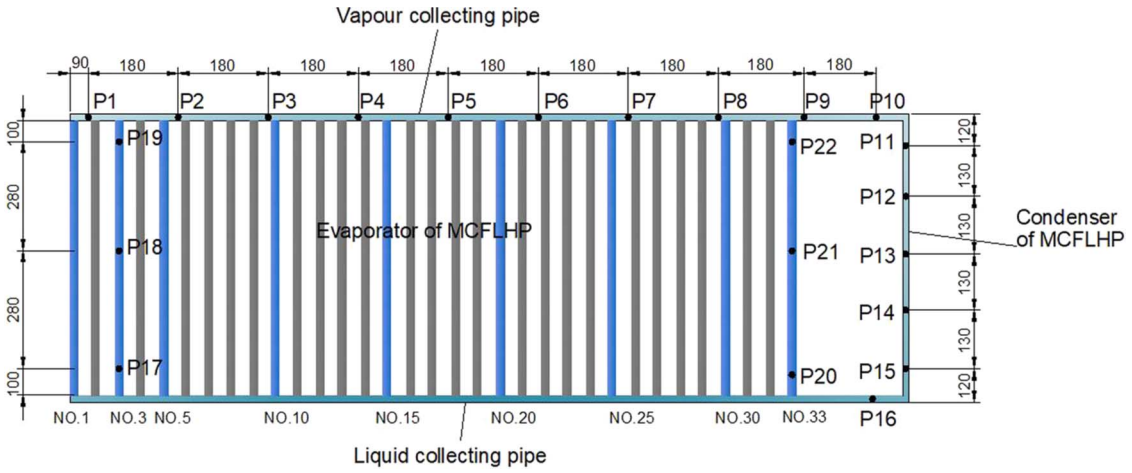

(a) Position of the temperature measuring points on the surface of the MCFLHP (Unit: mm)

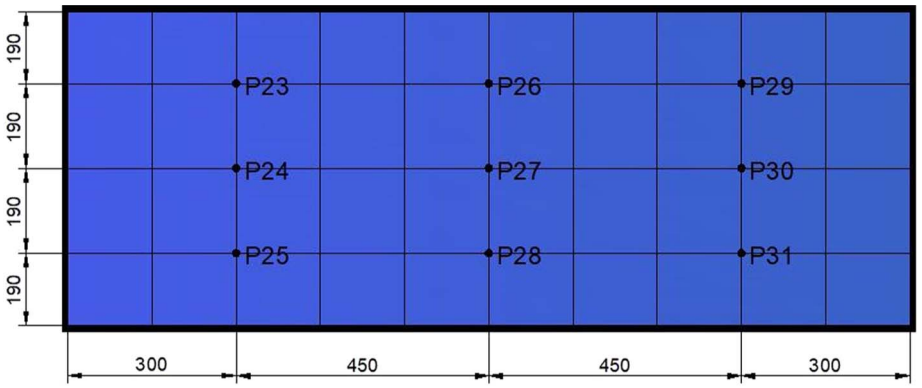

(b) Position of the solar radiation measuring points on surface of the PV panel (Unit: mm)

Figure 5. *Position of the measuring points.*

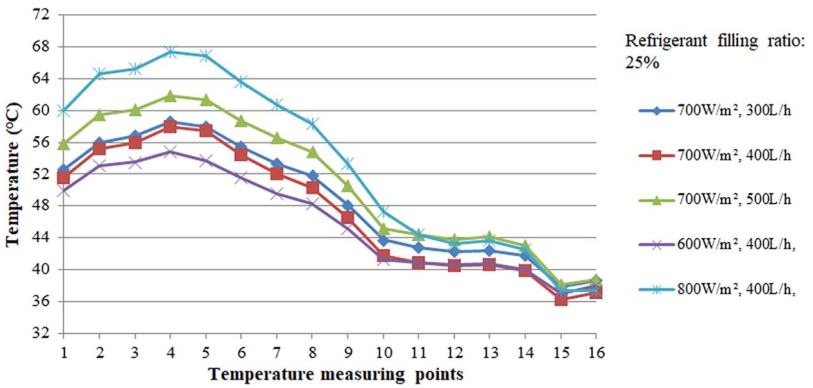

Figure 6. *Temperature variation of the MCFLHP under the refrigerant filling ratio of 25% condition (P1–P16)*

conditions (e.g. wind). It was also found that by controlling other two conditions, the thermal efficiency decreased with the increase of the refrigerant filling mass. This is because the increase in the refrigerant filling ratio would result in the increased dynamic viscosity and decreased specific heat ratio and eventually decreased thermal efficiency.

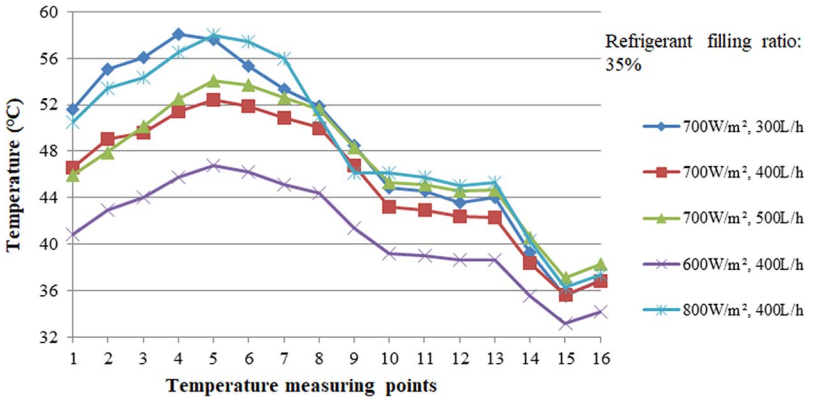

Figure 7. *Temperature variation of the MCFLHP under the refrigerant filling ratio of 35% condition (P1–P16).*

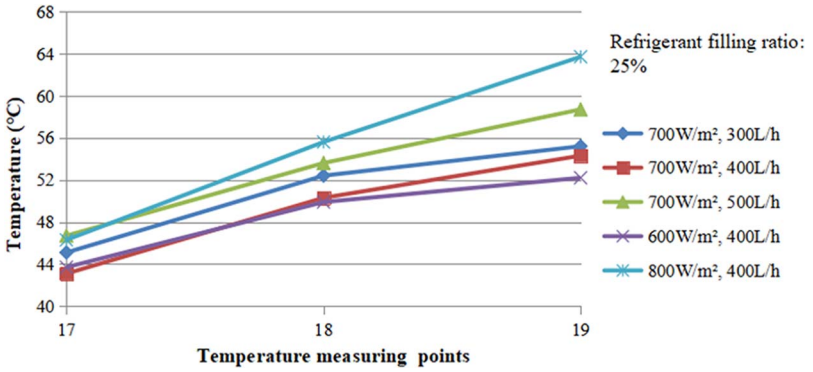

Figure 8. *Temperature variation of the MCFLHP under the refrigerant filling ratio of 25% condition (P17–P19 in the No. 3 heat pipe).*

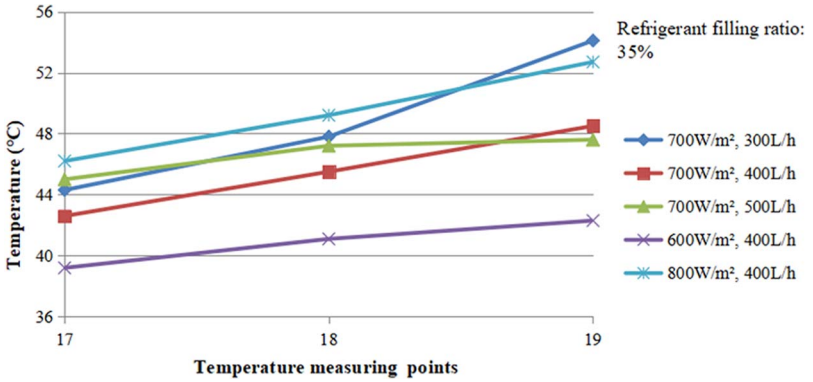

Figure 9. *Temperature variation of the MCFLHP under the refrigerant filling ratio of 35% condition (P17–P19 in the No. 3 heat pipe).*

5.3. Analysis of the system's electrical efficiency

The system's electrical efficiency was calculated from Equation (33) and is presented in Table 3. The power of electricity was calculated by considering voltage and current, which were recorded by Solar Power Controller MPPT. In comparing with the experimental conditions, it was noted that when the refrigerant filling ratio was 35%, the simulated radiation was 600 W/m² and the water flow rate of 400 L/h, the maximum average electrical efficiency of 8.4% could be achieved. The system's electrical efficiency decreased with the increase in the simulated radiation owing to the increase in the surface temperature of the PV panel, and the relationship between the average temperature of the PV panel and the electrical performance of the system is shown in Figure 12.

$$\eta_e = \frac{P_e}{Q_a} \times 100\% \tag{33}$$

5.4. Analysis of the system's total efficiency

The daily average total efficiency of the proposed system is also shown in Table 3. The total efficiency was also increased with the decrease in the refrigerant filling ratio, and the maximum daily

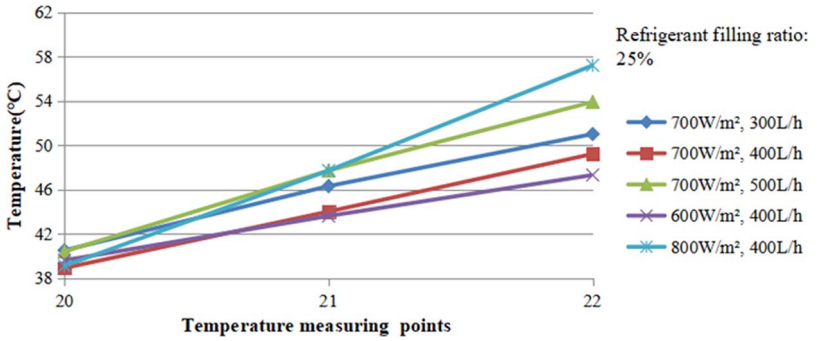

Figure 10. *Temperature variation of the MCFLHP under the refrigerant filling ratio of 25% condition (P20–P22 in the No. 33 heat pipe).*

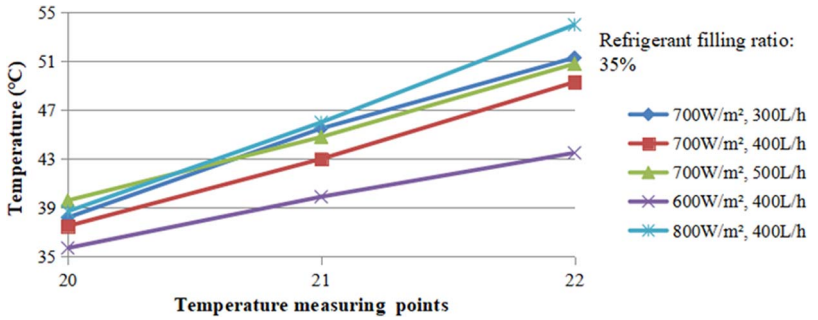

Figure 11. *Temperature variation of the MCFLHP under the refrigerant filling ratio of 35% condition (P20–P22 in the No. 33 heat pipe).*

Table 3. *Results of simulation and experiment.*

No.	Refrigerant filling ratio (%)	Simulated radiation (W/m²)	Water flow rate (L/h)	Inlet water temperature (°C)	Outlet water temperature (°C)	Tank water temperature increase—experiment (°C)	Thermal efficiency—experiment (%)	Thermal efficiency—simulation (%)	Error (%)	Electrical efficiency—experiment (%)	Total efficiency—experiment (%)	COP
1	25	700	300	21	24.8	3.8	38.9	43.4	10.3	7.4	46.3	3.88
2	25	700	400	21	25.3	4.3	43.8	48.7	10.0	7.5	51.3	4.23
3	25	700	500	21	25.2	4.2	42.8	48.7	12.1	7.5	50.3	4.16
4	25	600	400	21	24.3	3.3	39.7	45.6	12.9	8.3	48.0	3.51
5	25	800	400	21	25.5	4.5	40.0	42.6	6.2	7.0	47.0	4.44
6	35	700	300	21	24.3	3.3	34.0	36.9	7.8	7.1	41.1	3.50
7	35	700	400	21	25.0	4.0	40.8	43.5	6.2	7.8	48.6	4.08
8	35	700	500	21	24.7	3.7	37.9	41.0	7.6	7.6	45.5	3.85
9	35	600	400	21	24.2	3.2	38.6	42.0	8.2	8.4	47.0	3.46
10	35	800	400	21	25.2	4.2	37.4	40.4	7.4	7.1	44.5	4.26

average total efficiency of 51.3% could be achieved for the system operated under the refrigerant filling ratio of 25%, simulated radiation of 700 W/m² and water flow rate of 400 L/h.

5.5. Analysis of the system's coefficient of performance

The energy performance of the PV/T-MCFLHP system is evaluated by the coefficient of performance (COP). For the photovoltaic/thermal system, the electricity power generated by the PV panel should be converted into the equivalent thermal energy using the average electricity-generation efficiency, which is commonly at 38% [35]. The COP of the system could be then written as

$$\mathrm{COP} = \frac{Q_{\mathrm{cf}} + P_{\mathrm{e}}/0.38}{P_{\mathrm{pump}}} \tag{34}$$

The variations of the COP in different working conditions are shown in Table 3. The COP was found to be the highest at 4.44 when the refrigerant filling ratio is 25%, simulated radiation is 800 W/m² and water flow rate is 400 L/h. The COP increased with the decrease in the refrigerant filling ratio. This could be explained by highlighting that with the refrigerant filling ratio decreasing, the superheated vapour will flow to the condenser

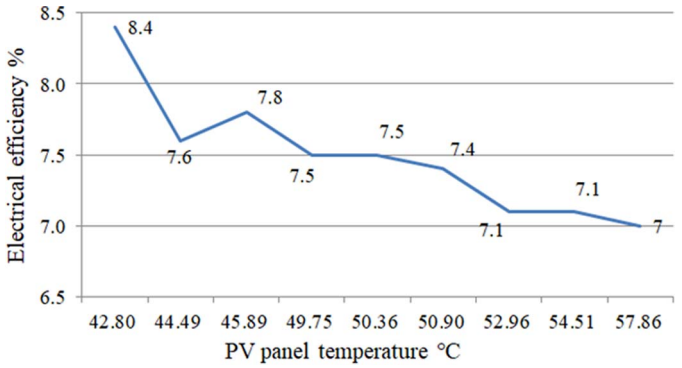

Figure 12. *Relationship between the electrical efficiency and the PV panel temperature.*

more quickly, resulting in more energy stored in the water tank and higher COP eventually. In the experiments, when under the same refrigerant filling ratio and the same water flow rate, the COP of the system increased with the increase in the simulated solar radiation. In the novel PV/T-MCFLHP system, water pump is the only energy-consumption equipment. In the meantime, as the simulated radiation increases, more heat was collected and recharged to the water tank, leading to increased COP as in Equation (34).

6. UNCERTAINTY ANALYSIS

The uncertainty of the system's thermal efficiency was demonstrated that the fractional uncertainties were influenced mainly by the refrigerant filling ratio, water flow rate and simulated radiation. Based on the errors of the instruments, the uncertainty values are calculated to be ±0.002 kg of electronic scales, ±10 L/h of float flow meter and ±6.5 W/m^2 of solar radiation simulator. According to Equation (35) [36], the uncertainties in the thermal efficiency were calculated to be 2.67%, meaning that the testing instruments had influence on the performance of the proposed system.

$$\frac{W_\eta}{\eta} = \left[\left(\frac{W_M}{M}\right)^2 + \left(\frac{W_V}{V}\right)^2 + \left(\frac{W_I}{I}\right)^2\right]^{\frac{1}{2}} \qquad (35)$$

7. CONCLUSION

In the paper, the novel photovoltaic/thermal (PV/T) system applying the micro-channel flat loop heat pipe (PV/T-MCFLHP) was proposed. In order to investigate the performance of the proposed system, the steady-state heat transfer simulation was carried out to analyse the performance of the system based on heat balance. The testing rig was also constructed, and the temperatures, e.g. PV panel and MCFLHP, were measured. The testing results were used to validate the simulation model under different working conditions, e.g. refrigerant filling ratio, simulated radiation and water flow rate. The comparison between the simulation and testing results indicated that the acceptable average error of 10.2% was found. It was also reported that the maximum thermal efficiency of 43.8% and the maximum total efficiency of 51.3% were determined for the proposed system operated under the conditions of the refrigerant filling ratio of 25%, simulated radiation of 700 W/m^2 and water flow rate of 400 L/h.

ACKNOWLEDGEMENTS

This work was financially supported by the National Key R&D Program of China (2016YFE0133300), Department of Science and Technology of Guangdong Province, China (2019A050509008), European Commission H2020-MSCA-RISE-2016 Programme (734340-DEW-COOL-4-CDC), European Commission H2020-MSCA-IF-2018 Programme (835778-LHP-C-H-PLATE-4-DC), EPSRC (EP/R004684/1) and Innovate-UK (TSB70507-481546).

REFERENCES

[1] Piratheepan M, Anderson TN. Performance of a building integrated photovoltaic/thermal concentrator for façade applications. *Sol Energy* 2017;**153**:562–73.
[2] Amasyali K, El-Gohary NM. A review of data-driven building energy consumption prediction studies. *Renew Sust Energ Rev* 2018;**81**:1192–205.
[3] Wang B, Cot LD, Adolphe L, Geoffroy S. Estimation of wind energy of a building with canopy roof. *Sustain Cities Soc* 2017;**35**:402–16.
[4] Vanaga R, Blumberga A, Freimanis R *et al.* Solar façade module for nearly zero energy building. *Energy* 2017;**157**:1025–34.
[5] Settino J, Sant T, Micallef C *et al.* Overview of solar technologies for electricity, heating and cooling production. *Renew Sust Energ Rev* 2018;**90**:892–909.
[6] Ahmed FE, Hashaikeh R, Hilal N. Solar powered desalination-technology, energy and future work. *Desalination* 2019;**453**:54–76.
[7] Yadav S, Panda SK, Tripathy M. Performance of building integrated photovoltaic thermal system with PV module installed at optimum tilt angle and influenced by shadow. *Renew Energ* 2018;**12**:11–23.
[8] Yang T, Athienitis AK. A review of research and developments of building-integrated photovoltaic/thermal (BIPV/T) systems. *Renew Sust Energ Rev* 2016;**66**:886–912.
[9] Chen F, Yin H. Fabrication and laboratory-based performance testing of a building-integrated photovoltaic-thermal roofing panel. *Appl Energ* 2016;**177**:271–84.
[10] Nagano K, Mochida T, Shimakura K *et al.* Development of thermal-photovoltaic hybrid exterior wallboards incorporating PV cells in and their winter performances. *Sol Energy Mater Sol Cells* 2003;**77**:265–82.
[11] Chen Y, Athienitis AK, Galal K. Modeling, design and thermal performance of a BIPV/T system thermally coupled with a ventilated concrete slab in a low energy solar house: part 1, BIPV/T system and house energy concept. *Sol Energ* 2010;**84**:1892–907.
[12] Chow TT, Chan ALS, Fong KF *et al.* Annual performance of building-integrated photovoltaic/water-heating system for warm climate application. *Appl Energ* 2009;**86**:689–96.
[13] Kim JH, Park SH, Kang JG, Kim JT. Experimental performance of heating system with building-integrated PVT (BIPVT) collector. *Energy Procedia* 2014;**48**:1374–84.
[14] Jouhara H, Chauhan A, Nannou T *et al.* Heat pipe based systems-advances and applications. *Energy* 2017;**128**:729–54.

[15] Moradgholi M, Nowee SM, Abrishamchi I. Application of heat pipe in an experimental investigation on a novel photovoltaic/thermal (PV/T) system. *Sol Energy* 2014;**107**:82–8.
[16] Long H, Chow TT, Ji J. Building-integrated heat pipe photovoltaic/thermal system for use in Hong Kong. *Sol Energy* 2017;**155**:1084–91.
[17] Li H, Sun Y. Performance optimization and benefit analyses of a photovoltaic loop heat pipe/solar assisted heat pump water heating system. *Renew Energy* 2019;**134**:1240–7.
[18] Chan CW, Siqueiros E, Ling-Chin J *et al.* Heat utilization technologies: a critical review of heat pipes. *Renew Sust Energy Rev* 2015;**50**:615–27.
[19] Yang X, Yan YY, Mullen D. Recent developments of lightweight, high performance heat pipes. *Appl Therm Eng* 2012;**33-34**:1–14.
[20] Deng Y, Zhao Y, Wang W *et al.* Experimental investigation of performance for the novel flat plate solar collector with micro-channel heat pipes array (MHPAFPC). *Appl Therm Eng* 2013;**54**:440–9.
[21] Hou L, Quan Z, Zhao Y *et al.* An experimental and simulative study on a novel photovoltaic-thermal collector with micro heat pipes array (MHPA-PV/T). *Energ Build* 2016;**124**:60–9.
[22] Chen Z, Tong X, Liu H *et al.* A design of the micro-plate loop heat pipe and development of the porous nickel capillary wick. *Procedia Eng* 2017;**205**:3931–7.
[23] Busse CA. Theory of the ultimate transfer of cylindrical heat pipes. *Int J Heat Mass Transf* 1973;**16**:169–86.
[24] Riffat SB, Zhao X, Doherty PS. Analytical and numerical simulation of the thermal performance of 'mini' gravitational and 'micro' gravitational heat pipe. *Appl Therm Eng* 2002;**22**:1047–68.
[25] Nemec P, Čaja A, Malcho M. Mathematical model for heat transfer limitations of heat pipe. *Math Comput Modell* 2013;**57**:126–36.
[26] Venkateswari R, Sreejith S. Factors influencing the efficiency of photovoltaic system. *Renew Sust Energ Rev* 2019;**101**:376–94.
[27] Kalogirou S. 2009. *Solar Energy Engineering: Process and Systems*. Elsevier, UK.
[28] Shukla A, Kant K, Sharma A, Biwole PH. Cooling methodologies of photovoltaic module for enhancing electrical efficiency: a review. *Sol Energy Mater Sol Cells* 2017;**160**:275–86.
[29] Cibira G. Relations among photovoltaic cell electrical parameters. *Appl Surf Sci* 2018;**461**:102–7.
[30] Karlsson HOE, Trägårdh G. Heat transfer in pervaporation. *J Membr Sci* 1996;**119**:295–306.
[31] Chernysheva MA, Vershinin SV, Maydanik YF. Operating temperature and distribution of working fluid in LHP. *Int J Heat Mass Transf* 2007;**50**:2704–13.
[32] Liu W, Kang J, Fu X *et al.* Analysis on heat resistance of the micro heat pipe with arteries. *Microelectron Eng* 2011;**88**:2255–8.
[33] Konev SV, Wang JL, Tu CJ. Characteristics of a heat exchanger based on a collector heat pipe. *Heat Recovery Systems and CHP* 1995;**15**:493–502.
[34] Mala GM, Li D, Dale JD. Heat transfer and fluid flow in micro-channels. *Int J Heat Mass Transf* 1997;**40**:3079–88.
[35] Huang BJ, Lin TH, Hung WC, Sun FS. Performance evaluation of solar photovoltaic/thermal systems. *Sol Energy* 2001;**70**:443–8.
[36] Nowzari R, Alabbagh LBY, Egelioglu F. Single and double pass solar air heaters with partially perforated cover and packed mesh. *Energy* 2014;**73**:694–702.